Optic Nerve Sheath as a Novel Mechanical Load on the Globe in Ocular Duction

Joseph L. Demer

Department of Ophthalmology, Stein Eye Institute; Biomedical Engineering Interdepartmental Program; Neuroscience Interdepartmental Program; Department of Neurology, University of California, Los Angeles, California, United States

Correspondence: Joseph L. Demer, Stein Eye Institute, 100 Stein Plaza, UCLA, Los Angeles, CA 90095-7002, USA; jld@jsei.ucla.edu.

Submitted: November 23, 2015
Accepted: March 12, 2016

Citation: Demer JL. Optic nerve sheath as a novel mechanical load on the globe in ocular duction. *Invest Ophthalmol Vis Sci*. 2016;57:1826–1838. DOI:10.1167/iovs.15-18718

Purpose. The optic nerve (ON) sheath's role in limiting duction has been previously unappreciated. This study employed magnetic resonance imaging (MRI) to demonstrate this constraint on adduction.

Methods. High-resolution, surface coil axial MRI was obtained in 11 normal adults, 14 subjects with esotropia (ET) having normal axial length (AL) < 25.8 mm, 13 myopic subjects with ET and mean AL 29.3 ± 3.3 (SD) mm, and 7 subjects with exotropia (XT). Gaze angles and ON lengths were measured for scans employing eccentric lateral fixation in which an ON became completely straightened.

Results. In all groups, ON straightening occurred only in the adducting, not abducting, eye. Adduction at ON straightening was 26.0 ± 8.8° in normal subjects, not significantly different from XT at 22.2 ± 11.8°. However, there was significant increase in comparable adduction in ET to 36.3 ± 9.3°, and in myopic ET to 33.6 ± 10.7° ($P < 0.04$). Optic nerve length at straightening was 27.6 ± 2.7 mm in normals, not significantly different from 28.2 ± 2.8 mm in ET and 27.8 ± 2.7 mm in XT. In myopic ET, ON length at straightening was significantly reduced to 24.0 ± 2.9 mm ($P < 0.002$) and was associated with globe retraction in adduction, suggesting ON tethering.

Conclusions. Large adduction may exhaust length redundancy in the normally sinuous ON and sheath, so that additional adduction must stretch the sheath and retract or deform the globe. These mechanical effects are most significant in ET with axial myopia, but may also exert traction on the posterior sclera absent strabismus or myopia. Tethering by the ON sheath in adduction is an important, novel mechanical load on the globe.

Keywords: optic nerve, myopia, magnetic resonance imaging, strabismus

Several sources of mechanical force acting on the eye have been intensively studied over the last century. The effects of intraocular pressure (IOP) exerted outward on the optic nerve (ON) head against intracranial pressure (ICP) have been extensively investigated[1–3]; however, investigations of both pressures have nearly universally neglected possible effects of ocular rotation from central position where the ON is typically examined clinically. The normal eye is capable of a wide range of rotations, reported in 100 normal subjects to average 51.6° adduction, 48.7° abduction, 37.6° supraduction, and 58.0° infraduction.[4] The ON must maintain anatomic continuity between the globe and orbital apex throughout this entire range of rotation. Remarkably, while prior studies have extensively considered the oculorotary forces exerted on the globe by the extraocular muscles (EOMs), existing biomechanical models of EOM loads have entirely neglected forces exerted by the ON, and all have modeled the sclera as an incompressible sphere.[5–10] The current report challenges both types of approaches with the observation from magnetic resonance imaging (MRI) that the ON, and especially the stiff connective tissue sheath that envelops the ON, exert appreciable mechanical force when the eye rotates into large-angle adduction, and suggests that this loading may both deform the globe, and perhaps even induce damaging stress on the afferent visual pathway that could contribute to glaucomatous optic neuropathy by imposing strain on the scleral canal, lamina cribrosa, and associated glial and vascular elements.

Biomechanical properties of sclera and lamina cribrosa may critically contribute to ON axonal damage, and thus to glaucoma,[2] as has been reviewed.[11,12] Strain (deformation) in the lamina cribrosa is heavily influenced by the sclera[3,12,13] such that effect of the normal range of variation in peripapillary scleral thickness equates to a 15 mm Hg IOP change.[14] Peripapillary sclera, composed of highly anisotropic fibers,[15] is subject to regional variation in nonlinearly viscoelastic properties dependent on loading rates and directions[12] that are particularly significant for large, transient deformations during eye movements.[11] To date, however, no consideration has been given to the possible role of normal eye movements or of the ON sheath in ON head deformation. Emphasis has rather been on IOP, and to a limited extent on translaminar pressure, the difference between IOP and ICP.[16–19]

Horizontal strabismus changes the relative angle between the eyes, and the resulting abnormal initial eye positions could result in greater than normal tension on the ON during further ocular duction. Globe elongation and nonspherical staphylomata associated with axial myopia might be associated with greater or lesser ON length, but would in any case require that ON path length change more than normal during ocular duction. This study therefore also included subjects with

exotropia (XT), and esotropia (ET) with or without concomitant axial myopia.

Methods

Subjects

A prospective MRI study of ocular motility and strabismus has been conducted continuously for the past 26 years with approval of the Institutional Review Board for Protection of Human Subjects of the University of California-Los Angeles, with written informed consent given prior to participation in conformity with the Declaration of Helsinki. Participating subjects included normal controls recruited by advertising, and strabismic patients recruited from the clinical practice of the author, who is an ophthalmologist specializing on ocular motility. All subjects underwent ophthalmic examination by the author, who also personally performed all MRI scanning. While the choices of particular imaging planes and gaze directions varied slightly among subjects according to specific experimental questions that evolved during this long-term study, the basic scanner hardware and imaging protocols were similar for the collection of digital image sets under controlled conditions in approximately 145 normal orthotropic and 650 strabismic subjects. From this prospective collection set were identified 44 individuals for inclusion in this study, including all subjects in whom there was availability of MRI of adequate quality in image planes and gaze directions relevant to the present study, as well as status as normal controls, esotropic and exotropic subjects, and axially high myopic subjects. All such eligible data sets in the overall collection for which one or both orbits could be analyzed were included for analysis of the measures described below. Subjects were excluded only for absence of axial MRI of interpretable quality in horizontal gazes at least including adduction, and for the presence of vertical strabismus.

Morphometry of the ON and ON sheath was performed in participating subjects using all T2-weighted images that had adequate quality to separately distinguish the ON, CSF gap, and ON sheath. Such features are generally not distinguishable on T1 imaging, so T1 images were excluded from the foregoing morphometric analysis.

Image Acquisition

Magnetic resonance imaging was performed of the orbits in each subject using surface coils and high-resolution technique with T1 or T2 weighting as previously described in detail.[20–23] Gadodiamide contrast was administered intravenously for some T1 imaging. Briefly, quasi-coronal imaging was also performed in planes perpendicular to the long axis of each orbit separately at 256 × 256 pixels with a square field of view of 8 cm, providing 312-μm in-plane resolution for 2-mm contiguous image planes (Fig. 1). During axial imaging parallel to the paths of the horizontal rectus EOMs, both orbits were imaged at 256 × 256 pixels with a square field of view of 10 to 11 cm, providing 390- to 430-μm in-plane resolution with 2-mm contiguous image planes (Fig. 2). Imaging was during monocular fixation of an afocal, illuminated target delivered by a fine optical fiber affixed to the transparent mask of the surface coil array (Medical Advances, Milwaukee, WI, USA) illuminated from the remote, opposite end by a red or blue light-emitting diode. It has been previously verified that the afocal monocular target does not induce vergence despite its roughly 20-mm proximity to the fixating eye. Targets were placed either centrally or at the farthest limits of abduction possible, limited by either subject ability to rotate the eye or by target occlusion by the surface coil itself. Because of anatomic or surface coil occlusion of nasally eccentric target fibers, target placement for the orbit imaged in adduction was generally for fixation by the abducting fellow eye. In some cases, even centered position of the fixating eye resulted in significant duction of the strabismic fellow eye.

Results Analyzed

Continuous variables analyzed included the axial length (AL) of the globe, anteroposterior length of the orbit, length of the ON at straightening, adduction angle at which ON straightening was observed, distance of posterior displacement of the globe in adduction, outer and inner dimensions of the ON sheath, thickness of the ON sheath, and thickness of the CSF gap between the ON and sheath. Qualitative observations were also made of ghosting in MRI images, the configuration of the globe, ON, and sheath in abduction and adduction, as well as ophthalmoscopic features such as tilting of the ON head, peripapillary atrophy, and presence of posterior staphylomata.

Image Analysis

Digital MRI images were quantitatively analyzed using the program ImageJ64 (W. Rasband, National Institutes of Health, Bethesda, MD, USA; http://rsb.info.nih.gov/ij/, 1997–2009 [in the public domain]). Axial globe length was taken as the distance from the anterior corneal surface to the retinal surface along a line perpendicular to the iris plane terminating at the foveal location temporal to the optic disc (Fig. 2), and measured in the axial image plane closest to the globe equator. Anteroposterior length of the orbit was taken as the distance between the common tendonous ring in the orbital apex and the most anterior edge of the bright fat pad along the nasal orbital wall, as assessed in the axial image plane closest to the center of the ON path (Fig. 2). Since central gaze visual direction is subjective and difficult to control precisely with an extremely proximate target, an objective measure of ocular direction obtained from axial MRI was used as a surrogate. Axial images were first digitally rotated so that the sagittal midline was aligned to scanner vertical. Gaze direction was determined in the axial image closest to the center of the pupil and ON as the angle between scanner vertical and that of a line drawn from the corneal apex through the pupil center, perpendicular to the plane of the iris, and continuing to the retinal surface temporal to the ON head (Fig. 2). While this anatomic criterion for gaze direction is unlikely to correspond exactly to subjective visual direction and while "straight ahead" gaze is subjective and somewhat arbitrary, the MRI approach to gaze direction employed here is robust for changes in horizontal duction angle, where it has been validated in a prior MRI study of convergence,[20] and would not introduce systematic bias.

Globe retraction was measured, in that axial MRI plane incorporating the maximum anteroposterior globe diameter, as the change in distance from globe centroid to an individually selected robust bony landmark that was clearly visible in all relevant gaze positions for the individual subject. While the choice of reference landmark varied among subjects according to their individual anatomy, it was always the same within each individual subject so that changes in the measured distance reflected actual changes in anteroposterior globe position relative to the bony orbit.

Ghost images due to unavoidable eye movements such as blinks were present in some images, as noted below. These ghosts were readily distinguishable from main images due to their faintness and blur, and were disregarded in quantitative measurements that were consequently interpretable. Images containing more than acceptable motion were considered uninterpretable, were not analyzed, and were usually immedi-

Investigative Ophthalmology & Visual Science

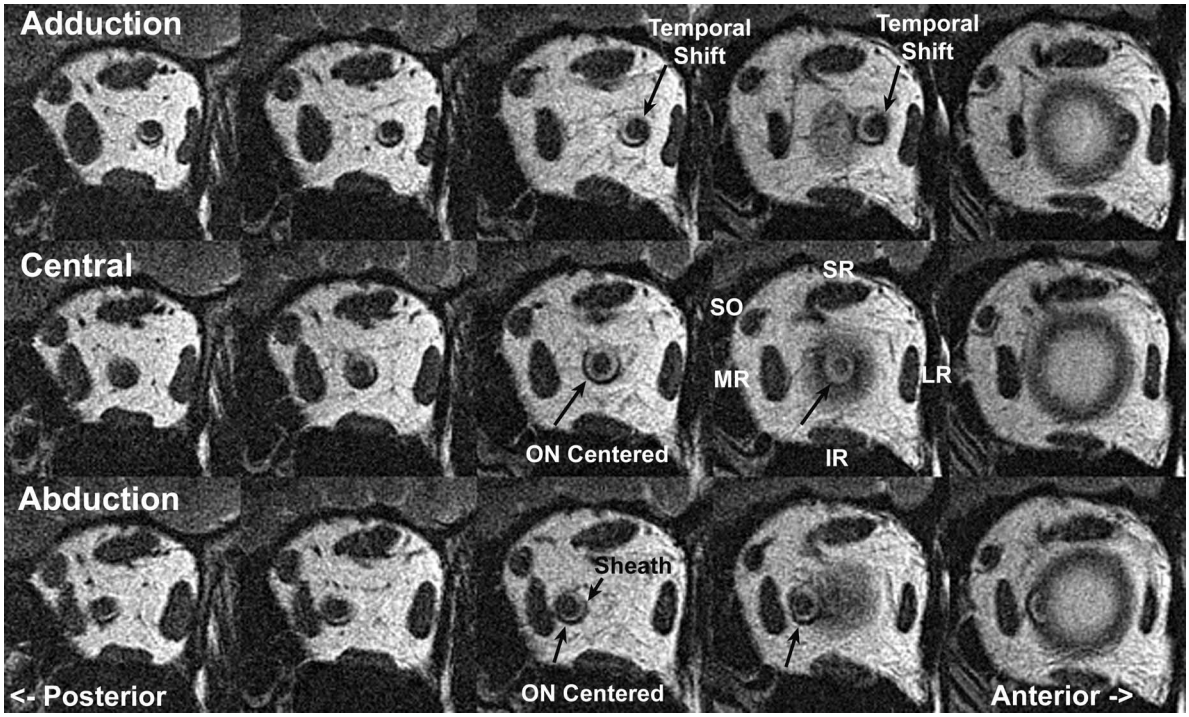

Figure 1. Quasi-coronal, T2-weighted MRI of left orbit of a representative normal subject in 2-mm-thick contiguous image planes. The *middle column* immediately posterior to the junction of the globe and optic nerve (ON) shows the maximum diameter of the ON sheath expansion, with a cuff of bright signal cerebrospinal fluid surrounding the ON within its sheath. This fluid space is reduced posteriorly (*left column*). The ON is centered within the sheath in central gaze (*middle row*) and abduction (*bottom row*), but shifts temporally in adduction (*top row*). IR, inferior rectus muscle; LR, lateral rectus muscle; MR, medial rectus muscle; SO, superior oblique muscle; SR, superior rectus muscle.

ately reacquired at acceptably higher quality at the time of scanning.

Optic nerve length was measured digitally in axial images closest to globe equator that were parallel to these EOMs (Fig. 2). Redundancy was considered to be ON length in excess of the shortest-distance, linear path. Because in most gaze positions the redundancy of the ON and its sheath often gave it a three-dimensionally sinuous path not lying in any specific plane, ON length was measured digitally from the orbital apex to the posterior sclera only in those gaze directions where ON path was straight in axial images. The straight-line length tool in ImageJ64 was employed for determination of ON length.

Quasi-coronal MRI was used to measure the inside and outside diameters of the ON sheath, and of the pial surface of the ON itself, in image planes from the posterior sclera to the orbital apex (Fig. 3). The gap between the pial surface of the ON and the inner surface of the ON sheath corresponds to the subarachnoid space. These structures were manually outlined using a free-form digital cursor in ImageJ64. Circular diameters were computed geometrically from measured cross-sectional areas assuming circular shapes; this approach is robust and has subpixel resolution. Circular symmetry with constant sheath and gap thickness was assumed for these features.

In cases of ET without associated unilateral axial high myopia, both eyes were analyzed. In cases of ET associated with unilateral high myopia, only the highly myopic eye was analyzed.

Statistics

Statistical analysis employed Student's *t*-test for continuous variables where sample size was appropriately large and approximately normally distributed, but Mann-Whitney non-parametric testing was used otherwise. Analysis of variance (ANOVA) was employed for multiple comparisons of continuous variables. Categorical distributions were analyzed using χ^2 testing. The 0.05 level was required for statistical significance, but because this was an exploratory study, specific levels are also reported when this level was appreciably surpassed. Analysis of anatomic MRI parameters was at the level of eyes rather than subjects, for efficiency and to avoid wastage of useful data.[24]

Replicability

Repeatability of ON length at straightening was evaluated by reevaluation of the original image data set by the author 3 to 12 months after the original analysis, without reference to the original values, and the second analysis is reported here. All ON lengths in adduction were remeasured using the original method and compared with original results using Bland-Altmann analysis, ANOVA, and Pearson correlation. It was not considered necessary to verify replicability for measurements of structures based upon MRI cross sections because such area-based measurements have subpixel resolution, are highly robust, and have been employed reliably for many years as indicators of structure and function in EOMs[22,25–31] and for structure of the ON.[32–34]

Results

Clinical and Demographic Characteristics

Clinical and demographic characteristics are listed in Table 1. Age varied significantly among subject groups (1-way ANOVA, $P = 0.006$), with the oldest subjects in the group that

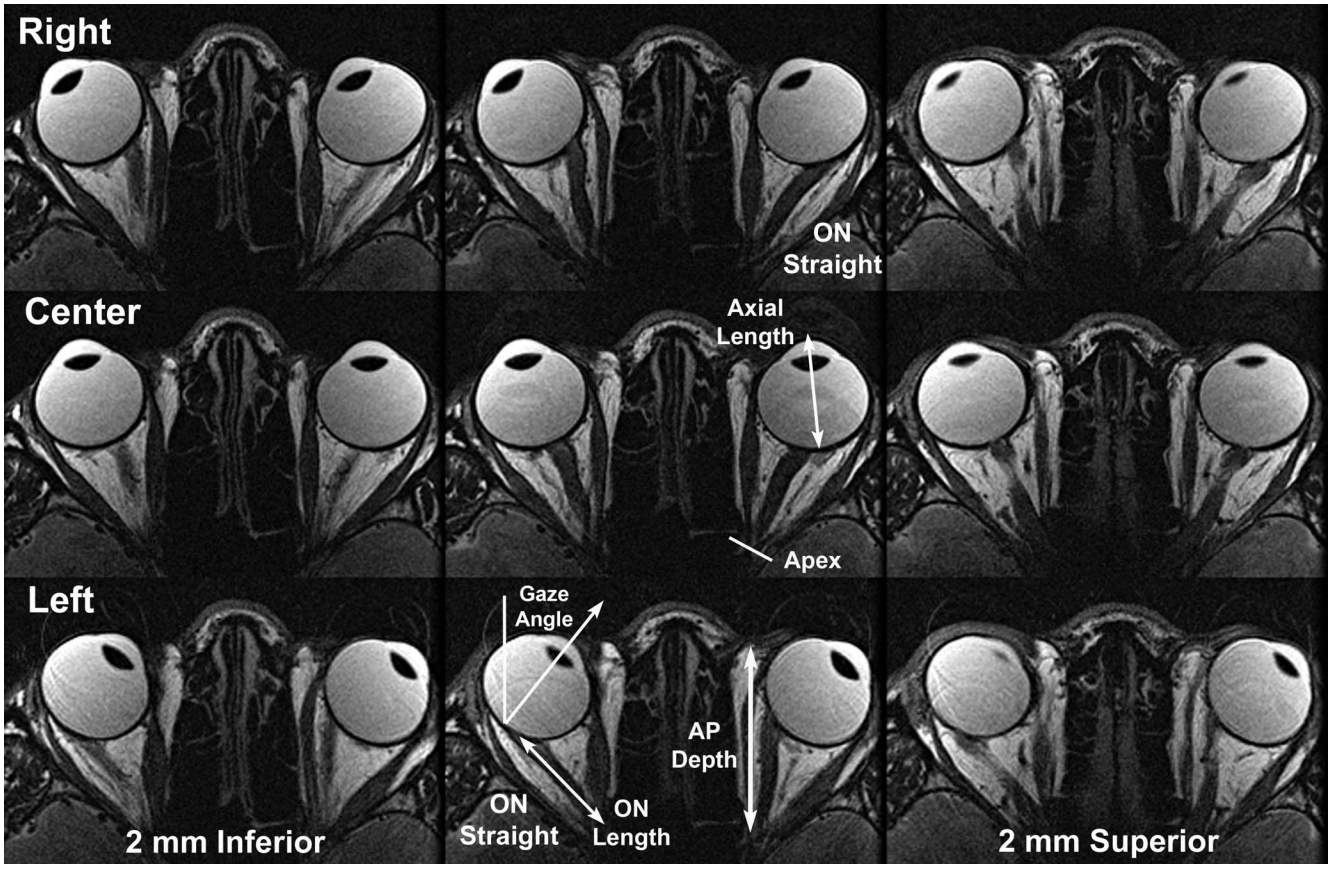

Figure 2. T2-weighted MRI of representative normal subject in contiguous, 2-mm-thick axial planes centered (*middle column*) on the optic nerve (ON) and including inferior and superior planes to illustrate the full diameter of the ON sheath. MRI was repeated in right (*top row*), center (*middle row*), and left (*lower row*) gazes. Note ON redundancy in central gaze and abduction, with the ON either sinuous within the same plane or between adjacent axial planes. However, in adduction of each eye, the ON is straightened and becomes apposed to the straight ON sheath surrounding it. ON length was measured from the posterior globe to the orbital apex as illustrated in the *lower image*. Anteroposterior (AP) orbit length was measured from the apex, the location of the common tendonous origin of the rectus muscles, to the anterior border of the orbital fat in the axial image plane closest to the center of the ON in central gaze.

exhibited both ET and axial myopia. χ^2 testing did not demonstrate significant differences in sex distribution among subject groups. Eleven control subjects had normal binocular alignment and visual function. Mean axial globe length measured by MRI in normal subjects was 23.7 ± 1.0 mm (SD), while the maximum value of normal AL was 25.7 mm. Fourteen subjects had ET and ALs in both eyes of no more than 25.7 mm that were considered not to represent axial myopia. Thirteen subjects had ET and AL of at least 25.7 mm, and so were considered to have axial high myopia. Mean AL in the group with ET and axial myopia was by design significantly greater than in all other groups as confirmed by parametric and nonparametric testing, but there were no significant differences in AL among other groups. Seven subjects had XT and 24.2 ± 1.5-mm mean AL; one eye in this group had 25.7-mm AL. Several strabismic subjects had previously undergone cataract surgery, and some had undergone prior strabismus surgery, although they nevertheless exhibited significant strabismus at the time of this study. Ophthalmoscopy showed that 12 of the highly myopic eyes had temporally tilted optic discs, and two more had peripapillary atrophy on the temporal disc margin; only one nonmyopic esotropic and one exotropic subject had temporal peripapillary atrophy.

Anatomy of ON and Sheath

There was remarkably little variation in the qualitative and average quantitative anatomy of the ON and sheath among normal and strabismic subjects. A consistent finding in subjects in all groups was fusiform expansion of the ON sheath immediately posterior to the globe–ON junction, with CSF present between the ON and the inside of the sheath that yields a bright signal on T2 imaging (Fig. 1). While exact dimensions of these structures are detailed in Table 2, immediately posterior to the globe the ON had roughly 3.5-mm diameter, the sheath was roughly 0.75-mm thick, and there was a 0.5- to 0.8-mm-thick subarachnoid space surrounding the ON within the sheath that contains CSF. Outside diameter of the ON sheath ranged from a minimum of 4 mm to a maximum of 8 mm in the most extreme cases, with the subarachnoid CSF gap ranging from zero to 1.6 mm. The ON was usually centered within the sheath in central gaze and abduction (Fig. 1, middle and lower rows), but shifted to the nasal side of the sheath in adduction, where it typically contacted the inner surface of the sheath (Fig. 2, upper row). Kruskal-Wallis nonparametric statistical testing demonstrated no differences among subject groups for any of the quantitative parameters of the ON and sheath listed in Table 2 ($P > 0.24$ for all).

Investigative Ophthalmology & Visual Science

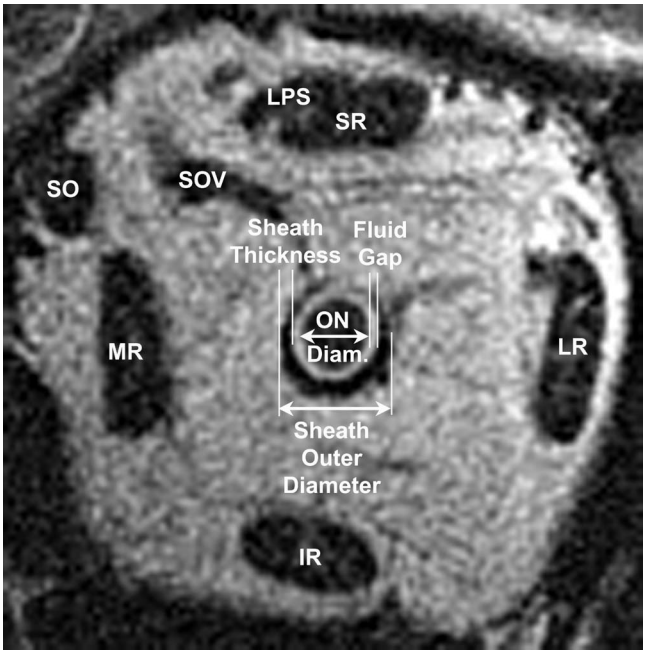

FIGURE 3. Quasi-coronal, T2 MRI of normal left orbit demonstrating measurements of the immediately retrobulbar optic nerve diameter (ON diam.), ON sheath outer diameter, sheath thickness, and cerebrospinal fluid gap (subarachnoid space). Diameters of circular structures were inferred from cross-sectional areas to achieve subpixel resolution, and circular symmetry with constant sheath and gap thickness was assumed. IR, inferior rectus muscle; LPS, levator palpebrae superioris; LR, lateral rectus muscle; MR, medial rectus muscle; SO, superior oblique muscle; SOV, superior ophthalmic vein.

Adduction in Normal Subjects

Axial plane MRI in normal subjects indicates the reason for shift of the ON toward the temporal edge of its sheath in adduction: The sheath exhausts its length redundancy and in this position exerts traction against the sclera, which pulls the taut sheath into contact with the ON. This effect, which is generally absent in abduction, is illustrated in Figure 2. Also evident in Figure 2 is the straightening of the ON and sheath in adduction.

Measurement of ON length in axial image planes is impossible when the ON is redundant, because length redundancy permits the ON to be sinuous both within and between adjacent planes. However, when the ON has become straight, it is constrained to a linear path whose length can readily be measured in axial planes placed to parallel the ON and long axis of the orbit. Length of the ON, from the common tendonous ring in the orbital apex to the globe, was recorded only in cases when the ON was straight, and this occurred only in adduction. As adduction progressively increased, the ON remained straight, as illustrated for a normal control subject in Figure 4A, and for an esotropic subject with axial high myopia in Figure 4B.

Adduction in Subjects With ET and Axial High Myopia

Since fixation in adduction was generally by the abducting fellow eye (due to target occlusion by the nose and surface coil), the angle of adduction was greater in esotropic and less in exotropic subjects. This is illustrated in Figure 5 for a moderately high myopic (spherical equivalent −9.00 diopters [D], AL 25 mm in each eye) subject with 55Δ ET in central gaze who exhibited marked ON straightening in adduction and MRI artifacts suggestive of involuntary motion. Such motion artifacts were frequently observed when either ON became straight and were seldom observed in central gaze.

Straightening of the ON in adduction was particularly prominent in esotropic subjects with axial high myopia, hence elongated globes with ALs exceeding 25.7 mm. Not only were ON straightening and movement artifacts prominent in adduction, but the anterior surface of the adducting eye, to a greater degree than the globe centroid, frequently retracted into the orbit. This is illustrated for the 54-year-old highly myopic subject in Figure 6 whose refraction is −26.5 D in the right and −22.5 D in the left eye; in adduction each globe's rotational center appeared to shift toward the globe–ON junction, rather than globe center, as the adducting globe retracted. The subject in Figure 6 had 29.2-mm axial globe length for the right and 29.7 mm for the left eye, with obviously oval globe shape constituting diffuse posterior staphylomata bilaterally.

Exotropia

Straightening of the ON was also observed in XT without axial myopia, albeit typically with less adduction than in ET, and without obvious retraction of the ocular surface. This is illustrated in Figure 7 for a 39-year-old subject whose refraction is mildly myopic at −3.00 D in the right and −2.50 D in the left eye. The lower left portion of this figure also shows the temporal shift of the ON within the sheath in adduction as temporal redundancy in the sheath was lost during straightening.

Globe Retraction

Posterior displacement, here termed retraction, of the anterior ocular surface in adduction would always correspond to posterior shift of the globe centroid if the globe were perfectly spherical. Since the cornea has a smaller radius of curvature than the sclera, even the normal globe is not exactly spherical, so there will be some difference between shifts in anteropos-

TABLE 1. Clinical and Demographic Characteristics

	N		Sex		Age, y		Axial Length, mm		Strabismus Angle, Δ	
Subject Group	Subjects	Orbits	Female	Male	Mean	SD	Mean	SD	Mean	SD
Normal control	11	14	5	6	38	18	23.7	1.0	N/A	N/A
Esotropic	14	25	7	5	48	19	23.4	1.2	41	21
Esotropic/myopic	13	21	10	4	56†	13	28.9*	2.8	48	32
Exotropic	7	13	3	4	37	21	24.5	1.5	34	22

Axial length values are means for eyes included. All other values are reported for individual subjects.
* Axial length significantly greater than in all other groups at $P < 0.0001$.
† Esotropic subjects with axial high myopia were significantly older than controls ($P < 0.02$), but no other age differences were significant.

Investigative Ophthalmology & Visual Science

Table 2. Retrobulbar Anatomic Dimensions in Central Gaze

	Control, $N = 18$		Esotropic, Nonmyopic, $N = 23$		Esotropic, Myopic, $N = 20$		Exotropic, $N = 11$	
Measurement, mm	**Mean**	**SEM**	**Mean**	**SEM**	**Mean**	**SEM**	**Mean**	**SEM**
Optic nerve diameter	3.55	0.07	3.63	0.05	3.61	0.12	3.45	0.09
Fluid gap thickness	0.59	0.04	0.66	0.06	0.53	0.14	0.76	0.08
Sheath thickness	0.74	0.02	0.77	0.02	0.78	0.04	0.73	0.04
Sheath outer diameter	6.16	0.12	6.44	0.11	6.32	0.33	6.00	0.16

N orbits. SEM, standard error of the mean. None of the measurements differed significantly by subject group ($P > 0.24$ for all).

terior centroid position and shifts in position of the ocular surface. Nevertheless, the anteroposterior position of the entire globe's area centroid in the equatorial axial MRI plane was considered to represent a robust measure of whole-eye position. Axial imaging was available in all three positions (central gaze, levoversion, and dextroversion) in some subjects in each group where these could all be obtained, as limited by total imaging time and subject cooperation; the numbers of subjects are listed in Figure 8. From these complete axial imaging sets, the changes from central gaze in the anteroposterior position of each eye relative to the same cranial landmark are plotted for abduction and adduction in each subject group in Figure 8. Normal and exotropic subjects exhibited no significant globe retraction in abduction or adduction. However, nonaxially myopic subjects with ET exhibited significant retraction averaging 1.00 ± 0.93 mm in adduction (median 1.14 mm, $P = 0.012$, 1-sample *t*-test against zero). Myopic subjects with XT exhibited a trend toward anterior globe displacement (proptosis) in abduction and posterior displacement (retraction) in adduction; while neither of these shifts differed significantly from zero by nonparametric Kruskal-Wallis testing, the difference in globe centroid position between abduction and adduction was significant ($P = 0.022$).

Globe centroid position shifts with horizontal duction were much larger than the median in some esotropic subjects with axial high myopia. These ranged from almost 3-mm proptosis in abduction to 4.5-mm retraction in adduction. However, while some of this apparent shift may have been due to geometric artifacts of nonspherical globes, the centroid method is more conservative than measurement of the anterior corneal surface, as seen for the example in Figure 6. While that subject did not undergo central gaze imaging and so did not contribute to the data of Figure 8, similar analysis comparing abduction versus adduction in each eye demonstrated no change in anteroposterior position of either globe centroid for that individual.

Adduction Angle for ON Straightening

The adduction angle at which ON straightening was observed is plotted for all groups of subjects in Figure 9. Statistical comparisons are 2-tailed *t*-tests assuming unequal variance. While adduction angle was similar at 22° to 26° in normal and exotropic subjects, it was significantly greater in axially myopic esotropic subjects at approximately 33° ($P < 0.005$), and significantly greater still in nonmyopic esotropic subjects at approximately 36° ($P < 0.05$).

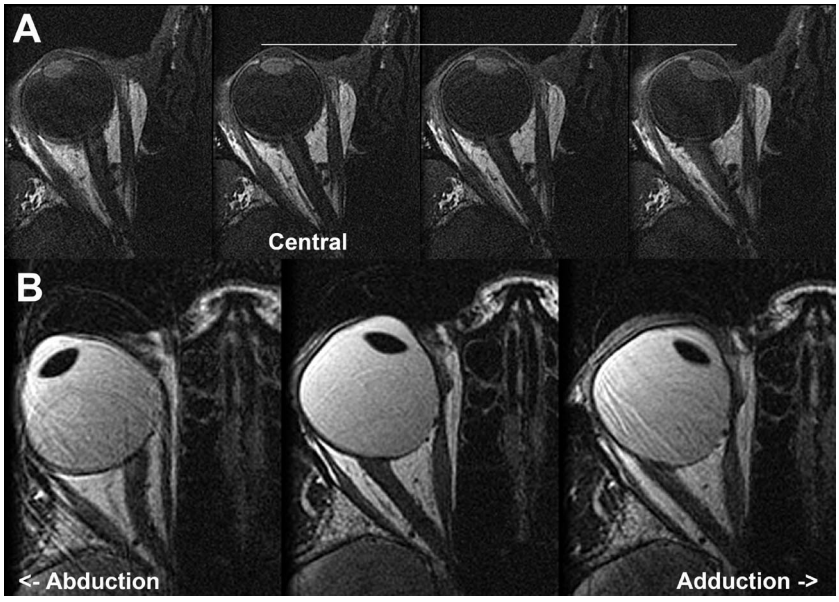

Figure 4. Axial MRI illustrating progressive straightening of the optic nerve (ON) from its sinuous course in abduction at *left* to progressively greater adduction in the *right columns*. (**A**) T1 sequence with gadodiamide contrast in orthotropic normal subject. The *white horizontal line* denotes the anterior corneal surface. Note that progressive adduction from the *third image from left* (ON length 28.0 mm, 11.5° adduction) is associated with slight globe surface retraction in large adduction (*upper right*, ON length 28.9 mm, 25.6° adduction). (**B**) T2 fast spin echo sequence in esotropic subject with axial high myopia demonstrating persistence of ON straightening during progressively increasing adduction at the *lower center* (ON length 24.6 mm, 19.0° adduction) and *lower right* (ON length 25.0 mm, 32.4° adduction). The myopic globe is nonspherical.

Investigative Ophthalmology & Visual Science

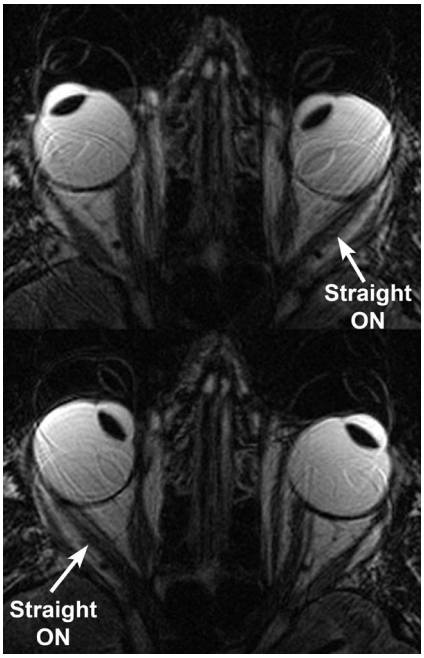

FIGURE 5. Axial MRI in right (*top*) and left (*bottom*) gazes showing optic nerve (ON) straightening in the adducting eye of moderately myopic subject who had 55Δ esotropia in central gaze. Ghost images of the sclera, cornea, and lens visible within the vitreous cavity indicate movement artifacts presumably due to involuntary eye movements induced by ON traction in the adducting eye.

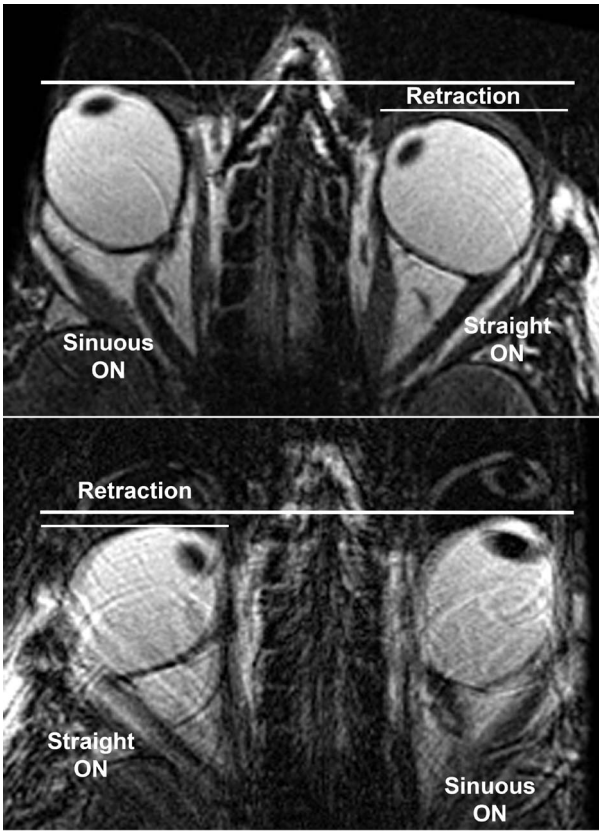

FIGURE 6. Axial MRI in highly axially myopic, esotropic subject. Note that when the left optic nerve (ON) straightened in adduction during right gaze (*top*), the anterior surface of the left globe underwent approximately 4-mm retraction. When the right ON straightened in right eye adduction during left gaze (*bottom*), the right globe underwent slightly less retraction. Ghost images, particularly in the *lower image*, represent motion artifacts due to involuntary eye motion typically observed during globe retraction.

Length of the ON

Length of the ON for which straightening was observed is plotted for all groups of subjects in Figure 10. In orthotropic control subjects and subjects with XT and ET without axial high myopia, ON length at straightening was similar at approximately 28 mm. However, in esotropic subjects with axial high myopia, ON length was significantly less than in the foregoing at 24.0 ± 0.6 (SEM) mm ($P < 0.002$).

Replicability Analysis

After an interval of 3 to 12 months from initial analysis, the author performed replicate analysis of ON length at which straightening was observed in adduction. Since there were no statistically significant differences between mean values of initial and repeat ON length measurements for any of the four subject groups ($P > 0.1$), data were pooled for further statistical analysis. The Pearson correlation coefficient for repeat measurement was 0.692 ($P < 10^{-8}$). The Bland-Altman method showed a bias of 0.605 mm (2.2%) between initial and repeat analyses; this bias is much smaller than the significant effect in Figure 10.

Orbital Length

Orbital length was approximately 41 mm and did not vary significantly among the four subject groups (ANOVA, $P > 0.05$). Data on orbital length and straight ON length were pooled for all subjects in all groups to ascertain any possible association between these measures, as plotted in Figure 11. Linear regression demonstrated significant correlation ($P = 0.0025$) between orbit and straight ON lengths, but with orbit length accounting for only 11% of the variance in ON length. The slope of the linear relationship was 0.304 ± 0.097 (SD), implying that ON length increases on average by only approximately 30% of orbit length.

DISCUSSION

The present study extends a long history of use of MRI morphometry of orbital tissues to make inferences about their relative mechanical states, beginning with the pioneering work of Miller culminating in discovery of the pulley system,[35] continuing to the general use of morphometry to infer other constraints on EOM paths,[27,36,37] and recently to contractility of whole EOMs[29,38,39] and their compartments.[22,31,40] Imaging cannot currently demonstrate force levels, constituting mechanical stress, within EOMs and other orbital tissues, but imaging in multiple gaze positions can directly demonstrate mechanical strain, the deformation and displacement resulting from mechanical force. Imaging of tissue displacement and deformation is most specific for noncontractile connective tissues that cannot actively generate tension. The sclera, ON, and ON sheath are such passive tissues whose mechanical strains represent morphologic readouts of the forces acting upon them that are quantitatively interpretable if the constitutive mechanical properties (e.g., elastic moduli) of the tissues are known.

While the ON exhibits a redundant and sinuous intraorbital course in central gaze, the present demonstration by MRI that

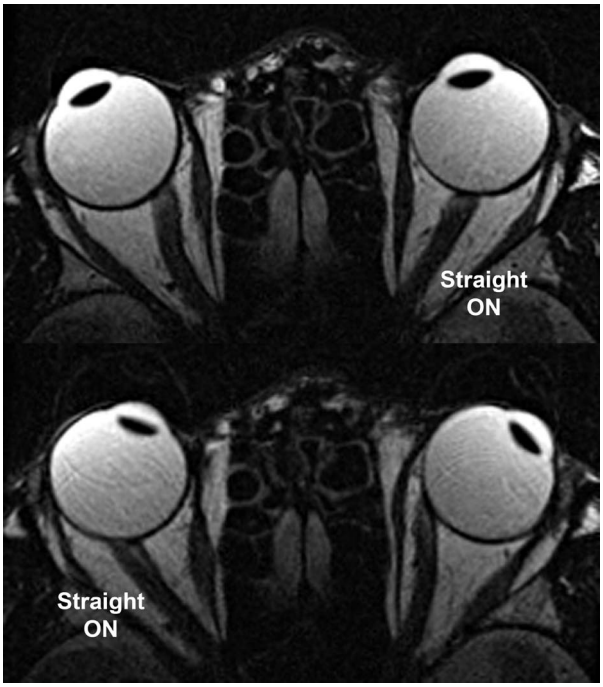

FIGURE 7. Axial MRI in mildly myopic, exotropic subject. The optic nerve (ON) straightened in adduction, while having a sinuous path in abduction for each eye. Note in *lower left* the temporal shift of the ON within the sheath in adduction as temporal redundancy in the sheath was lost during straightening.

the ON path becomes straightened well within the 52° physiologic range of adduction[4] therefore suggests that the ON and sheath exert tractional force on the globe when adduction surpasses the angle of straightening. While the current study provides only indirect morphologic evidence for such tractional force that cannot at present be specified quantitatively, the present imaging of the geometry of the globe and ON during gaze shifts is highly suggestive of traction by the latter that is a nonlinear function of duction angle. The ON cannot exert much if any tension on the globe in eye positions where ON path is sinuous and redundant, because non-zero tension would pull the ON path straight within the fluid environment of the orbital fat. Since ON straightening in adduction is demonstrable in normal as well as in strabismic subjects, it is likely that tractional force exerted by the ON is a normal mechanical load on the medial rectus (MR) muscle, albeit a load that contributes in a nonlinear and presumably threshold manner only for larger adduction angles. Since the ON is attached to the approximately spherical globe well posterior to its normal center of rotation that only roughly corresponds to its geometric center,[26] tractional force on the globe by the ON sheath would shift the globe's rotational center posteriorly, progressively retracting the globe with further adduction. The extent to which this effect occurs would depend upon the elastic compliance of the ON and its sheath; if these structures were completely inelastic, then upon ON straightening, the center of globe rotation would fully shift to the globe–ON junction itself. The geometric configuration seen in each adducting eye in Figure 4 suggests that globe rotation about a point near the globe–ON junction might actually occur at extreme adduction angles in some

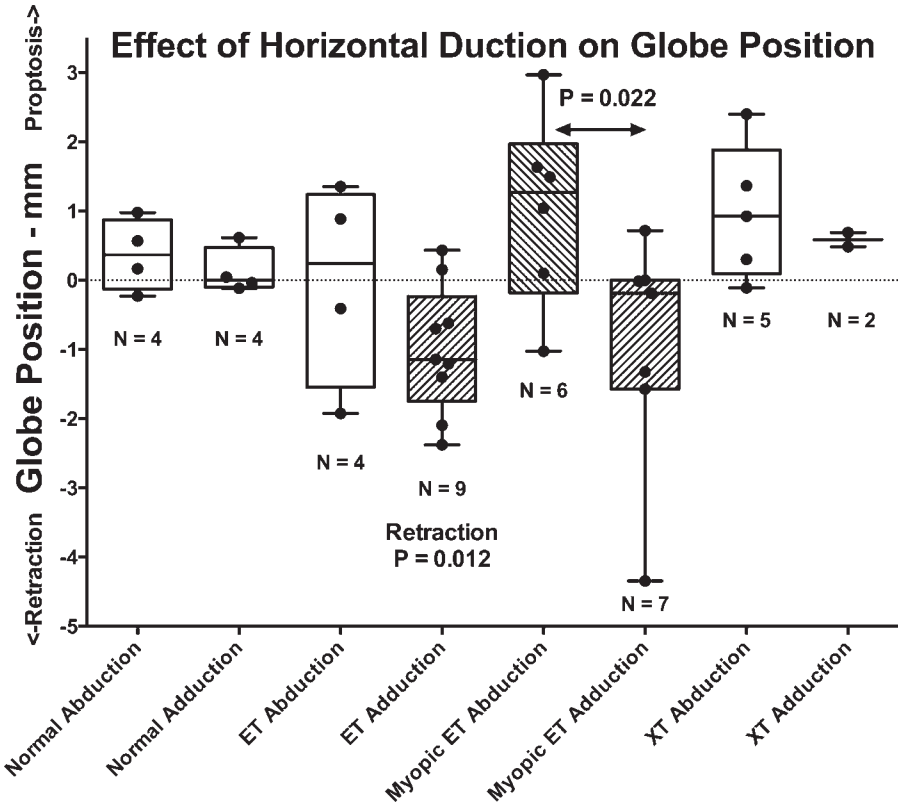

FIGURE 8. Box and whiskers plot showing effect of horizontal duction on anteroposterior position of the equatorial globe centroid as measured in axial MRI. Retraction in nonmyopic subjects with esotropia (ET) was significant by 1-sample *t*-testing against zero. Anteroposterior centroid position was significantly more posterior in adduction than abduction in axially myopic subjects with ET ($P = 0.022$ by Kruskal-Wallis test). *Rectangles* represent interquartile range with median indicated by *horizontal bar*. Whiskers represent maxima and minima. Individual observations are indicated by *filled circles*.

Investigative Ophthalmology & Visual Science

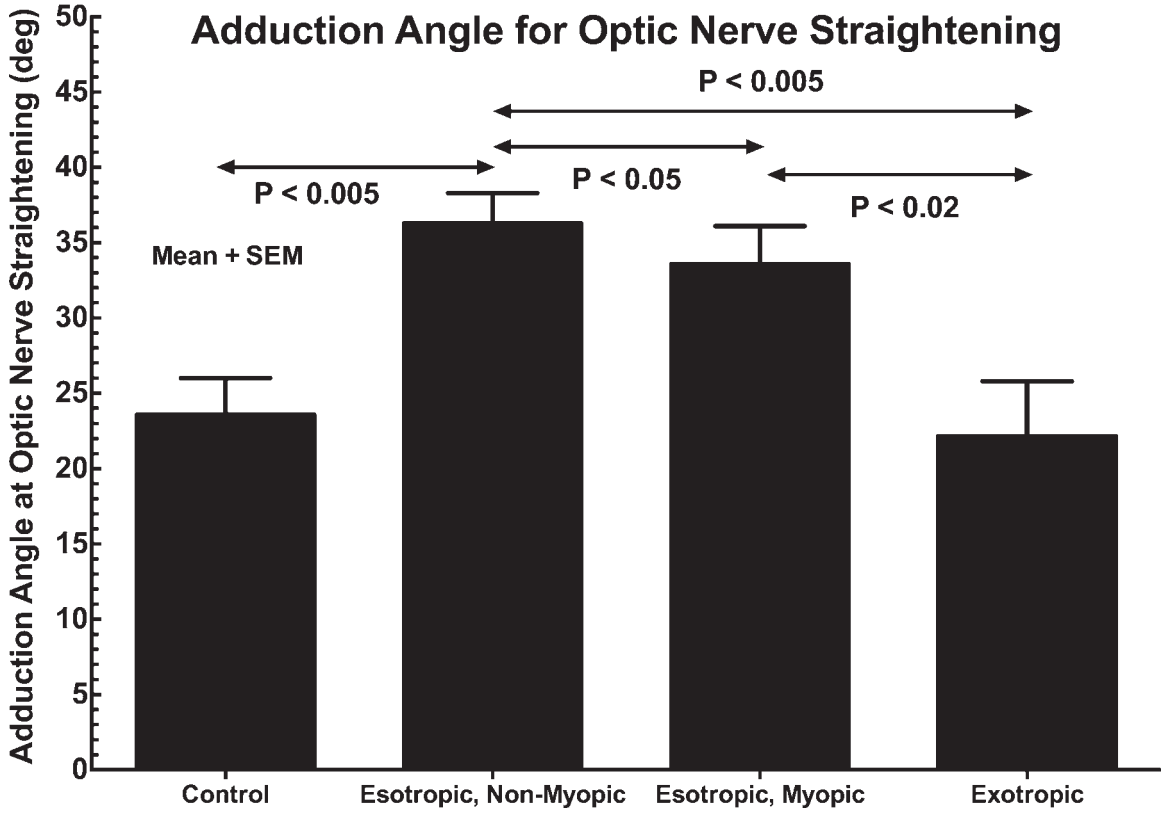

Figure 9. Adduction angle at which optic nerve straightening was observed in control and strabismic subjects. While the angle did not differ significantly between control and exotropic subjects, adduction angle was significantly greater in esotropic subjects but significantly more so in those who were nonmyopic. Statistical comparisons are 2-tailed *t*-tests assuming unequal variance. SEM, standard error of mean.

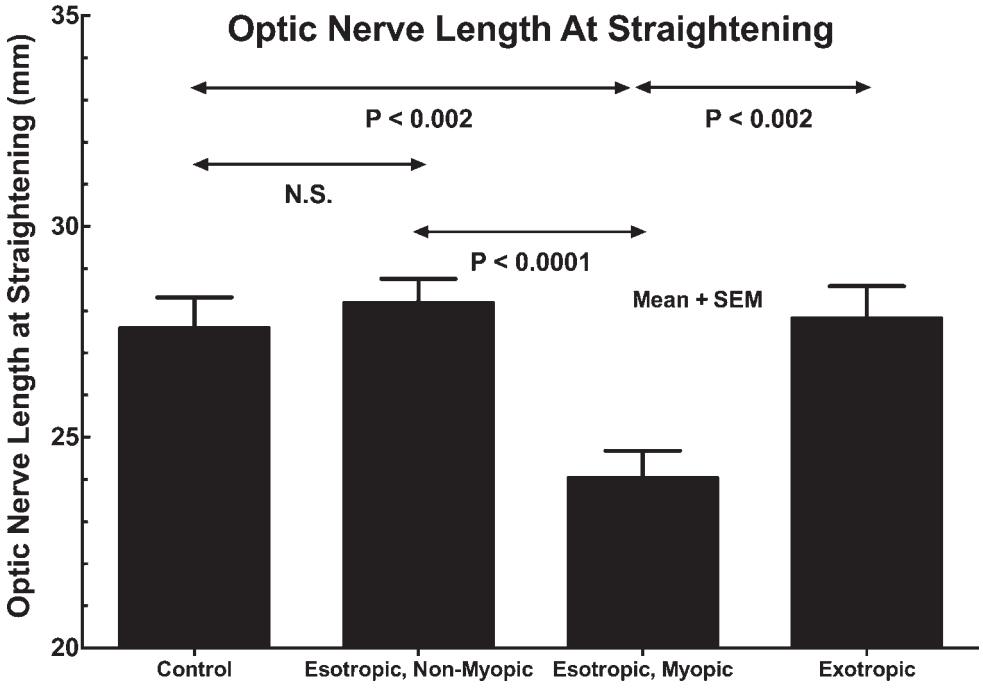

Figure 10. Length of the optic nerve (ON) at which straightening was observed in adduction. While ON length did not differ significantly between control and exotropic subjects, the ON was significantly shorter in esotropic subjects. Statistical comparisons are 2-tailed *t*-tests assuming unequal variance. Control and exotropic subjects did not differ significantly. SEM, standard error of mean.

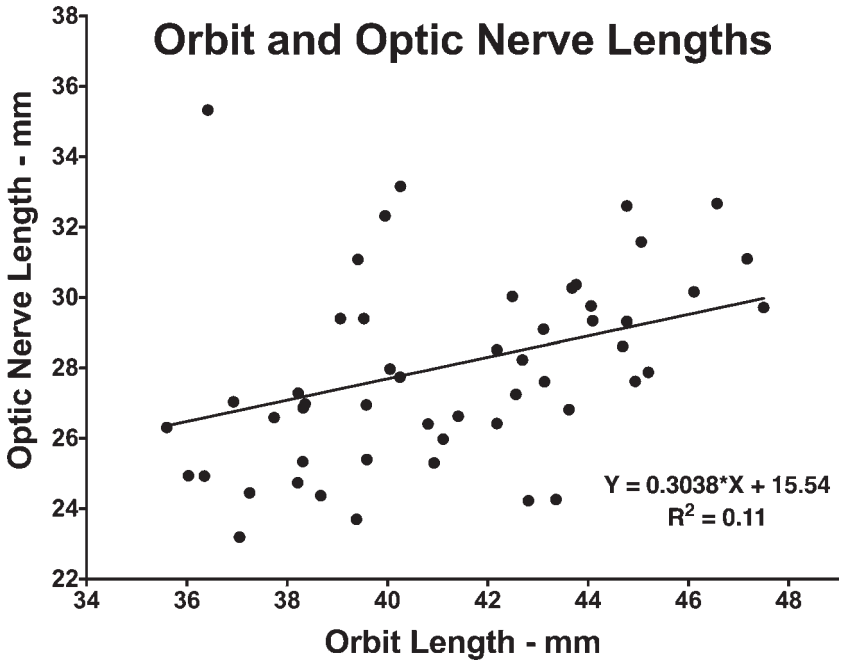

Figure 11. Relationship between anteroposterior length of the orbit and length of the optic nerve (ON) at straightening based upon pooled data for all subjects in all groups. While the linear correlation is significant ($P = 0.0025$), orbit length accounts for only 11% of the variance in ON length.

circumstances, producing appreciable globe retraction. Moreover, the ON elongation evident in Figure 4 for adduction exceeding the angle of ON straightening represents strain of 0.4 to 0.9 mm, which is approximately 1% to 3%. If the stiffness of the ON and sheath could be determined, then incremental strain observed by MRI could be simply interpreted as actual tissue tension in quantitative units of force.

The present axial MRI images showing globe retraction during ON straightening in adduction suggest that the ON and its sheath are indeed highly stiff compared to the tissues supporting the globe's anteroposterior position. Imaging in moderately and markedly axially myopic globes shows globe retraction in adduction, as predicted above (Figs. 6, 7); these results are consistent with relatively high stiffness of the ON and ON sheath. Moreover, the axial MRI in this study suggest that the main mechanical effect that develops upon ON straightening does not originate from the ON per se, but from its enveloping sheath. The retrobulbar ON and its sheath exhibited highly uniform morphometry across all subject groups (Table 2), even in axial myopes where the optic disc may appear larger than normal on ophthalmoscopy. This is probably due to retrobulbar coalescence of a normal number of axons from the optic disc. In the immediately retrobulbar region, the ON sheath has a diameter approximately 1.2 mm greater than the ON, so that CSF fills the resulting subarachnoid space around the ON centered within a bulbous enlargement of the retrobulbar sheath. In larger angles of adduction, the temporal region of the ON sheath is pulled straight, flattening it against the ON, and shifting the CSF to the nasal side of the ON where the sheath remains locally redundant (Figs. 1, 2). The MRI thus suggests that the mechanical constraint on adduction is due to tension in the temporal portion of the ON sheath, exerting its force very focally at the temporal edge of the ON's scleral canal. The ON itself is probably protected from tensile loading by the surrounding ON sheath that resists the load.

There are currently few or no published data on the biomechanical properties of the ON and its sheath in humans. However, data obtained from tensile loading of fresh bovine tissues provides general insight. Young's modulus is a measure of the elastic stiffness of isotropic material. The Young's modulus of bovine ON is similar to that of peripapillary sclera at approximately 5 MPa; the Young's modulus of peripheral sclera is approximately 3-fold higher at approximately 14 MPa (Shin A, et al. *IOVS* 2016;57:ARVO E-Abstract 3563). But, at approximately 45 MPa, the Young's modulus of ON sheath is some 9-fold greater than for peripapillary sclera (Shin A, et al. *IOVS* 2016;57:ARVO E-Abstract 3563). The high modulus of ON sheath is consistent with its postulated role in protecting the ON from tensile loading. Biomechanical calculations from finite element analysis using these data from the bovine eye suggest high tractional force concentration at the temporal margin of the ON's scleral canal, in the same region where peripapillary atrophy typically occurs and was present in most of the axially myopic subjects in the current study (Shin A, et al. *IOVS* 2016;57:ARVO E-Abstract 3563). Recent data suggest similar relationships for human tissues, and similar concentration of tractional ON sheath forces at the temporal edge of the ON's scleral canal (Shin A, et al. *IOVS* 2016;57:ARVO E-Abstract 3563). These forces correspond to temporal tilting of the ON head and to posterior staphylomata, nonspherical distortions of globe shape commonly present in axial myopes as exemplified in Figure 4 (lower) and Figure 6. Optical coherence tomography (OCT) demonstrates instantaneous posterior displacement of the ON head and temporal peripapillary sclera in adduction but not abduction even in normal subjects (Chang MY, et al. *IOVS* 2016;57:ARVO E-Abstract 4710).

Could any other structure besides the ON and its sheath provide the counterforce to the MR that results in globe retraction in adduction? The lateral rectus (LR) muscle might at first glance be supposed for such a role, except that in adduction the relaxed LR has a highly curved path bowed away from the globe that indicates that is not under much tension,[36] certainly suggesting that its tension could not balance that of the straightened, contracting MR muscle.

Anteroposterior orbit length does not vary significantly with the presence of strabismus or axial myopia, and is highly variably related to ON length at straightening. On average, ON length increases by only approximately 30% of orbit length (Fig. 11). Therefore, other geometric features of the globe and orbit account for ON straightening in adduction and absence of such straightening in abduction. Since the orbits are angled temporally and the ON inserts nasal to the fovea, the globe–ON junction travels over a larger arc from central gaze into adduction than it does from central gaze into abduction. Thus it is geometrically plausible that ON straightening was observed here in adduction in all subjects, but not in abduction. Straightening of the ON was observed at approximately 23° adduction in control and exotropic subjects (Fig. 9). Since normal subjects can achieve greater adduction angles,[4] the ON, its sheath, and other orbital tissues probably deform during larger normal adductions, perhaps along with some globe retraction. The unique load placed upon the normal MR muscle by ON sheath tension may be one reason why MR contractility exceeds contractility of the LR muscle,[22] which is not similarly burdened. Esotropic subjects exhibited ON straightening at significantly greater adduction angles than normal, at angles exceeding 30° (Fig. 9). While the current study demonstrates the ON to be straightened at these larger angles in ET, it is probable that the straightening first developed at smaller angles and persisted for the larger adductions (Fig. 4). That interpretation is supported by data on lengths of the ON at which straightening occurred (Fig. 10). In normal and exotropic subjects, ON length at straightening was approximately 28 mm (Fig. 10). In subjects with ET and axial high myopia, however, ON length at straightening was significantly less than in the foregoing groups at about 24 mm. This ON shortening has a particularly important effect in esotropic subjects with axial high myopia, where the globe–ON junction is more remote than normal from globe center. In central gaze the 29-mm mean AL of the highly myopic esotropic subjects would displace the globe–ON junction approximately 5 mm posterior to that for 24-mm normal AL; this is in correspondence with the roughly 4 mm shorter ON in these myopes. However, the distances fail to match in adduction. In adduction, the larger radius of a spherical myopic globe requires that the globe–ON junction travel over a roughly 10% longer arc than for normal control eyes. The shorter ON implies that in axially myopic subjects, ON straightening probably occurs at smaller adduction angles and induces greater ON sheath traction on the globe than occurs in subjects with normal AL. These factors would be further exaggerated in axial myopes with ET, and especially in the presence of posterior staphylomata as illustrated in Figure 6. Thus, more so than in emmetropic or exotropic people, most adducting saccades and quick phases of vestibular and optokinetic nystagmus could lead to ON straightening in esotropic people who have axial myopia.

Causality cannot be inferred from the present data, which beg several questions about the length of the ON and its sheath in relationship to globe and orbit dimensions. Factors that might regulate ON length are unknown. The data in Figure 11 suggest that anteroposterior orbital length is not a major factor. It is conceivable that ON length might be regulated to obtain a minimum to correspondingly minimize axonal conduction time to the brain; were this so, the ON might become adaptively shortened in axial myopia. Alternatively, if the ON first happened to be short for some other reason, ON traction on the posterior sclera in adduction, repeated numerous times during adducting saccades and quick phases over many years, might lead to scleral deformation with globe elongation and posterior staphyloma formation. The short ON might therefore be one mechanical cause of axial high myopia, a factor to be considered in the pathogenesis of this increasingly common disorder.[41] This possibility merits further study in axially myopic subjects who do not have ET, because the present investigation did not include myopes without strabismus.

Even transient traction by the ON sheath on the globe could be harmful to vision. Acute proptosis causing ON tethering is known to "tent" the globe at an angle whose apex is at the globe–ON junction; a "tenting angle" reduced by ON traction to less than 120° has been considered to be an acute emergency necessitating surgical correction for salvage of vision.[42] This urgency is unlikely to be applicable to staphylomatous, myopic globes such as in Figure 6, where the presumably chronic tenting angle may be seen to be 110° to 120° in both eyes. However, the known phenomenon of acute globe tenting due to ON traction motivates consideration of less acute effects on the peripapillary sclera and lamina cribrosa (LC) through which ON axons must travel from the retina to the brain. The present data suggest that every large adducting eye movement may be associated with focal, tensile loading of the temporal peripapillary sclera by the ON sheath. These forces could be transmitted to the LC, producing ON axonal damage, and thus be one of the mechanical contributors to glaucoma.[2,11,12] Peripapillary sclera, composed of highly anisotropic fibers,[15] features regional variation in nonlinearly viscoelastic properties dependent on loading rates and directions[12] that may be significant for large, transient deformations during saccades.[11]

Young children seldom exhibit an ON cup and virtually never ON head tilting,[43] peripapillary atrophy, or axial myopia[44]; these features develop with age[45] and become common in myopia,[46,47] which is progressive and now exceeds 95% prevalence among young adults in Asia.[41] Axial myopia is associated with posterior staphyloma, peripapillary choroidal thinning, and peripapillary atrophy,[45] particularly temporally,[45,48] where the choroid contributes blood supply to the prelaminar ON.[49] Peripapillary atrophy,[50] most prominently at the temporal ON margin,[51] is frequent with glaucoma[52–53] and is progressive with age,[50] myopia,[54] and glaucoma progression,[52,55–58] where it correlates with the topography[59] and degree of ON damage and visual field loss.[58–60] Peripapillary atrophy is closely associated with ON head tilt and torsion, both of which correlate with visual field defects in normal-tension but not high-tension glaucoma.[61] As seen in the current study, ON tilt is mainly temporal and/or inferior and corresponds to LC tilting and nerve fiber layer thinning.[62] The nerve fiber layer defects associated with normal-tension glaucoma are wider and closer to the fovea in concurrent myopia,[63] where OCT suggests that scleral canal deformation causes optic neuropathy.[64] It is therefore possible that glaucomatous optic neuropathy might arise not only from IOP pushing out against the scleral canal and LC, but that importantly when IOP is not high, also from traction as the ON sheath pulls out against these structures when the EOMs have adducted the eye sufficiently to exhaust ON sheath redundancy. These strains on peripapillary sclera probably occur dynamically, particularly during saccades. While EOM forces are distributed broadly against their wide scleral insertions, the ON sheath insertion is small, concentrating the counterforce to produce high local strain. There is recent supporting evidence from OCT that larger angles of adduction, but not adduction, deepen the optic cup, and thin and posteriorly displace the choroid at the temporal border of the optic disc in normal subjects (Chang MY, et al. *IOVS* 2016;57:ARVO E-Abstract 4710).

Study Limitations

This was an initial, exploratory study designed to introduce the novel concept that the ON and its sheath may constitute a

mechanical load on globe rotation, and to suggest some settings in which the phenomenon may be more prominent. Since a relatively small number of subjects were studied with a relatively narrow range of pathologies who were not closely matched by age or for a variety of other factors, strong conclusions are not supportable concerning possible age and sex effects or axial myopia in the absence of coexisting ET. Data on ON length was in most cases collected in only one position of adduction, so incremental strain on the straight ON could be determined in only a few cases. Of course, it would be biomechanically informative about quantitative ON and ON sheath stiffness to collect such data at varying angles of adduction past the point of straightening in more subjects.

Conclusions

In large-angle adduction, redundancy of the ON and its sheath is exhausted, straightening their normally sinuous paths so that they exert tractional force on the globe that appears in some cases sufficient to cause globe retraction. This effect appears to be due to the reaction force of the MR muscle exerted against the relatively stiff ON sheath. While present in normal subjects, ON straightening is more prominent in people with ET associated with axial high myopia where the ON itself is foreshortened yet experiences greater geometric ON path elongation due to abnormally great globe radius. Tethering in adduction by the ON and its sheath represents an important, yet novel, biomechanical constraint on ocular duction. This constraint is important not only to the understanding of ocular motility, but also to myopia and may represent a pressure-independent contribution to optic neuropathy in glaucoma. Detailed ex vivo biomechanical study of the ON, its sheath, and the peripapillary sclera, correlated with noninvasive in vivo studies, will be necessary to fully elucidate these phenomena and their relationship to aging in strabismus, myopia, and normal tension glaucoma. Additional data are also required on possible effects of age-related declines in the range of ocular duction,[65,66] which may interact with these pathologies and the ages at which they occur.

Acknowledgments

Supported by U.S. Public Health Service, National Eye Institute Grants EY008313 and EY000331, and an unrestricted grant from Research to Prevent Blindness. The author holds the Arthur L. Rosenbaum Professorship of Pediatric Ophthalmology.

Disclosure: **J.L. Demer**, None

References

1. Jonas JB, Wang N, Yang D, et al. Facts and myths of cerebrospinal fluid pressure for the physiology of the eye. *Prog Retin Eye Res*. 2015;46:67–83.
2. Burgoyne CF, Downs JC, Bellezza AJ, et al. The optic nerve head as a biomechanical structure: a new paradigm for understanding the role of IOP-related stress and strain in the pathophysiology of glaucomatous optic nerve head damage. *Prog Retin Eye Res*. 2005;24:39–73.
3. Girard MJ, Downs JC, Burgoyne CF, Suh JK. Peripapillary and posterior scleral mechanics–part I: development of an anisotropic hyperelastic constitutive model. *J Biomech Eng*. 2009;131:051011.
4. Gerling J, Lieb B, Kommerell G. Duction ranges in normal probands and patients with Graves' ophthalmopathy, determined using the Goldmann perimeter. *Int Ophthamol*. 1997; 21:213–221.
5. Robinson DA. A quantitative analysis of extraocular muscle cooperation and squint. *Invest Ophthalmol*. 1975;14:801–825.
6. Miller JM, Robinson DA. A model of the mechanics of binocular alignment. *Comput Biomed Res*. 1984;17:436–470.
7. Miller JM, Pavlovski DS, Shaemeva I. *Orbit 1.8 Gaze Mechanics Simulation*. San Francisco: Eidactics; 1999.
8. Porrill J, Warren PA, Dean P. A simple control law generates Listing's positions in a detailed model of the extraocular muscle system. *Vision Res*. 2000;40:3743–3758.
9. Warren PA, Porrill J, Dean P. Consistency of Listing's law and reciprocal innervation with pseudo-inverse control of eye position in 3-D. *Biol Cybern*. 2004;91:1–9.
10. Buchberger M, Kaltofen T, Priglinger S, et al. *SEE++ User Manual: Simulation Expert for Eyes*. Hagenberg, Austria: Upper Austrian Research GmbH; 2003.
11. Sigal IA, Ethier CR. Biomechanics of the optic nerve head. *Exp Eye Res*. 2009;88:799–807.
12. Downs JC. Optic nerve head biomechanics in aging and disease. *Exp Eye Res*. 2015;133:19–29.
13. Sigal IA, Flanagan JG, Tertinegg I, Ethier CR. Finite element modeling of optic nerve head biomechanics. *Invest Ophthalmol Vis Sci*. 2004;45:4378–4387.
14. Norman RE, Flanagan JG, Sigal IA, et al. Finite element modeling of the human sclera: influence on optic nerve head biomechanics and connections with glaucoma. *Exp Eye Res*. 2011;93:4–12.
15. Zhang L, Albon J, Jones H, et al. Collagen microstructural factors influencing optic nerve head biomechanics. *Invest Ophthalmol Vis Sci*. 2015;56:2031–2042.
16. Siaudvytyte L, Januleviciene I, Ragauskas A, et al. Update in intracranial pressure evaluation methods and translaminar pressure gradient role in glaucoma. *Acta Ophthalmol Scand*. 2015;93:9–15.
17. Jonas JB, Yang D, Wang N. Intracranial pressure and glaucoma. *J Glaucoma*. 2013;22(suppl 5):S13–S14.
18. Berdahl JP, Fautsch MP, Stinnett SS, Allingham RR. Intracranial pressure in primary open angle glaucoma, normal tension glaucoma, and ocular hypertension: a case-control study. *Invest Ophthalmol Vis Sci*. 2008;49:5412–5418.
19. Berdahl JP, Allingham RR. Intracranial pressure and glaucoma. *Curr Opin Ophthalmol*. 2010;21:106–111.
20. Demer JL, Kono R, Wright W. Magnetic resonance imaging of human extraocular muscles in convergence. *J Neurophysiol*. 2003;89:2072–2085.
21. Demer JL, Dusyanth A. T2 fast spin echo magnetic resonance imaging of extraocular muscles. *J AAPOS*. 2011;15:17–23.
22. Demer JL, Clark RA. Differential compartmental function of medial rectus muscle during converged and conjugate ocular adduction. *J Neurophysiol*. 2014;112:845–855.
23. Demer JL, Miller JM. Orbital imaging in strabismus surgery. In: Rosenbaum AL, Santiago AP, eds. *Clinical Strabismus Management: Principles and Techniques*. Philadelphia: WB Saunders; 1999:84–98.
24. Murdoch IE, Morris SS, Cousens SN. People and eyes: statistical approaches in ophthalmology. *Br J Ophthalmol*. 1998;82:971–973.
25. Clark RA, Miller JM, Demer JL. Displacement of the medial rectus pulley in superior oblique palsy. *Invest Ophthalmol Vis Sci*. 1998;39:207–212.
26. Clark RA, Miller JM, Demer JL. Three-dimensional location of human rectus pulleys by path inflections in secondary gaze positions. *Invest Ophthalmol Vis Sci*. 2000;41:3787–3797.
27. Kono R, Clark RA, Demer JL. Active pulleys: magnetic resonance imaging of rectus muscle paths in tertiary gazes. *Invest Ophthalmol Vis Sci*. 2002;43:2179–2188.

28. Demer JL, Clark RA, Kung J. Functional imaging of human extraocular muscles in head tilt dependent hypertropia. *Invest Ophthalmol Vis Sci*. 2011;52:3023–3031.
29. Clark RA, Demer JL. Functional morphometry of horizontal rectus extraocular muscles during ocular duction. *Invest Ophthalmol Vis Sci*. 2012;53:7375–7379.
30. Clark RA, Demer JL. Lateral rectus superior compartment palsy. *Am J Ophthalmol*. 2014;15:479–487.
31. Demer JL, Clark RA. Magnetic resonance imaging demonstrates compartmental muscle mechanisms of human vertical fusional vergence. *J Neurophysiol*. 2015;113:2150–2163.
32. Karim S, Clark RA, Poukens V, Demer JL. Quantitative magnetic resonance imaging and histology demonstrates systematic variation in human intraorbital optic nerve size. *Invest Ophthalmol Vis Sci*. 2004;45:1047–1051.
33. Demer JL, Clark RA, Engle EC. Magnetic resonance imaging evidence for widespread orbital dysinnervation in congenital fibrosis of extraocular muscles due to mutations in KIF21A. *Invest Ophthalmol Vis Sci*. 2005;46:530–539.
34. Demer JL, Clark RA, Lim KH, Engle EC. Magnetic resonance imaging evidence for widespread orbital dysinnervation in dominant Duane's retraction syndrome linked to the DURS2 locus. *Invest Ophthalmol Vis Sci*. 2007;48:194–202.
35. Miller JM. Functional anatomy of normal human rectus muscles. *Vision Res*. 1989;29:223–240.
36. Demer JL. Inflection in inactive lateral rectus muscle: evidence suggesting focal mechanical effects of connective tissues. *Invest Ophthalmol Vis Sci*. 2007;49:4858–4864.
37. Clark RA, Isenberg SJ, Rosenbaum SJ, Demer JL. Posterior fixation sutures: a revised mechanical explanation for the fadenoperation based on rectus extraocular muscle pulleys. *Am J Ophthalmol*. 1999;128:702–714.
38. Demer JL, Clark RA. Magnetic resonance imaging of human extraocular muscles during static ocular counter-rolling. *J Neurophysiol*. 2005;94:3292–3302.
39. Clark RA, Demer JL. Enhanced vertical rectus contractility by magnetic resonance imaging in superior oblique palsy. *Arch Ophthalmol*. 2011;129:904–908.
40. Clark RA, Demer JL. Differential lateral rectus compartmental contraction during ocular counter-rolling. *Invest Ophthalmol Vis Sci*. 2012;53:2887–2896.
41. Pan CW, Dirani M, Cheng CY, et al. The age-specific prevalence of myopia in Asia: a meta-analysis. *Optom Vis Sci*. 2015;92:258–266.
42. Dalley RW, Robertson WD, Rootman J. Globe tenting: a sign of increased orbital tension. *Am J Neuroradiol*. 1989;10:181–186.
43. Witmer MT, Margo CE, Drucker M. Tilted optic disks. *Surv Ophthalmol*. 2010;55:403–428.
44. Park HJ, Hampp C, Demer JL. Longitudinal study of optic cup progression in children. *J Pediatr Ophthalmol Strabismus*. 2011;48:151–156.
45. Samarawickrama C, Mitchell P, Tong L, et al. Myopia-related optic disc and retinal changes in adolescent children from Singapore. *Ophthalmology*. 2011;118:2050–2057.
46. Vongphanit J, Mitchell P, Wang JJ. Population prevalence of tilted optic disks and the relationship of this sign to refractive error. *Am J Ophthalmol*. 2002;133:679–685.
47. Kim TW, Kim M, Weinreb RN, et al. Optic disc change with incipient myopia of childhood. *Ophthalmology*. 2012;119:21–26, e1–e3.
48. Gupta P, Cheung CY, Saw SM, et al. Peripapillary choroidal thickness in young Asians with high myopia. *Invest Ophthalmol Vis Sci*. 2015;56:1475–1481.
49. Hayreh SS. Blood supply of the optic nerve head and its role in optic atrophy, glaucoma, and oedema of the optic disc. *Br J Ophthalmol*. 1969;53:721–748.
50. Savatovsky E, Mwanza JC, Budenz DL, et al. Longitudinal changes in peripapillary atrophy in the ocular hypertension treatment study: a case-control assessment. *Ophthalmology*. 2015;122:79–86.
51. Jonas JB, Nguyen XN, Gusek GC, Naumann GO. Parapapillary chorioretinal atrophy in normal and glaucoma eyes. I. Morphometric data. *Invest Ophthalmol Vis Sci*. 1989;30:908–918.
52. Jonas JB, Martus P, Horn FK, et al. Predictive factors of the optic nerve head for development or progression of glaucomatous visual field loss. *Invest Ophthalmol Vis Sci*. 2004;45:2613–2618.
53. Xu L, Wang Y, Yang H, Jonas JB. Differences in parapapillary atrophy between glaucomatous and normal eyes: the Beijing Eye Study. *Am J Ophthalmol*. 2007;144:541–546.
54. Nakazawa M, Kurotaki J, Ruike H. Longterm findings in peripapillary crescent formation in eyes with mild or moderate myopia. *Acta Ophthalmol*. 2008;86:626–629.
55. Uhm KB, Lee DY, Kim JT, Hong C. Peripapillary atrophy in normal and primary open-angle glaucoma. *Korean J Ophthalmol*. 1998;12:37–50.
56. Rockwood EJ, Anderson DR. Acquired peripapillary changes and progression in glaucoma. *Graefes Arch Clin Exp Ophthalmol*. 1988;226:510–515.
57. Budde WM, Jonas JB. Enlargement of parapapillary atrophy in follow-up of chronic open-angle glaucoma. *Am J Ophthalmol*. 2004;137:646–654.
58. Uchida H, Ugurlu S, Caprioli J. Increasing peripapillary atrophy is associated with progressive glaucoma. *Ophthalmology*. 1998;105:1541–1545.
59. Jonas JB, Naumann GO. Parapapillary chorioretinal atrophy in normal and glaucoma eyes. II. Correlations. *Invest Ophthalmol Vis Sci*. 1989;30:919–926.
60. Jonas JB. Clinical implications of peripapillary atrophy in glaucoma. *Curr Opin Ophthalmol*. 2005;16:84–88.
61. Park HY, Lee KI, Lee K, et al. Torsion of the optic nerve head is a prominent feature of normal-tension glaucoma. *Invest Ophthalmol Vis Sci*. 2015;56:156–153.
62. Hwang YH, Yoo C, Kim YY. Myopic optic disc tilt and the characteristics of peripapillary retinal nerve fiber layer thickness measured by spectral-domain optical coherence tomography. *J Glaucoma*. 2012;21:260–265.
63. Kim JM, Park KH, Kim SJ, et al. Comparison of localized retinal nerve fiber layer defects in highly myopic, myopic, and non-myopic patients with normal-tension glaucoma: a retrospective cross-sectional study. *BMC Ophthalmol*. 2013;13:67.
64. Akagi T, Hangai M, Kimura Y, et al. Peripapillary scleral deformation and retinal nerve fiber damage in high myopia assessed with swept-source optical coherence tomography. *Am J Ophthalmol*. 2013;155:927–936.
65. Clark RA, Isenberg SJ. The range of ocular movements decreases with aging. *J AAPOS*. 2001;5:26–30.
66. Shechtman D, Shallo-Hoffmann J, Rumsey J, et al. Maximum angle of ocular duction during visual fixation as a function of age. *Strabismus*. 2005;13:21–26.

Investigative Ophthalmology & Visual Science